IRANIAN JOURNAL OF PHYSICS RESEARCH

Iranian Journal of Physics Research, Vol. 12, No. 3, 2012

Effects of the sintering temperature on the flux-pinning mechanism and the activation energy of malic-acid doped MgB_2

S R Ghorbani[1, 3], M Bashi[2], M S A Hossain[3] and G Peleckis[3]

1. Department of Physics, Ferdowsi University of Mashhad, Mashhad, Iran
2. Department of Physics, Hakim Sabzevari University, Sabzevar, Iran
3. Institute for Superconducting and Electronic Materials, University of Wollongong, Wollongong, New South Wales 2522, Australia
E-mail: ghorbani@sttu.ac.ir

(Received 29 May 2011 , in final from 26 November 2012)

Abstract

The flux-pinning mechanism and activation energy of 10 wt % malic acid-doped MgB_2 were investigated by measuring of the critical current density and resistivity as a function of magnetic field and temperature. A crossover field, B_{sb}, was observed from the single vortex to the small vortex bundle pinning regime. For the sintered sample, the temperature dependence of $B_{sb}(T)$ at low temperature is in good agreement with the $\delta\ell$ pinning mechanism, i.e., pinning associated with charge-carrier mean free path fluctuation. The activation energy was decreased by increasing the magnetic field and increased by increasing sintering temperature.

Keywords: Malic-acid doped MgB_2, Critical current density, Flux-pinning mechanism, Activation energy

1. Introduction

MgB_2 superconductor has been studied extensively by many research groups around the world since its discovery [1]. Because MgB_2 has a simple crystal structures, large coherence length, high critical current density, and a lack of weak-link grain boundaries, it is a good candidate for new applications, such as large-scale engineering applications and electronic devices [2]. However, the critical current density, J_c, of MgB_2 drops rapidly in high magnetic field. Therefore, research approaches have been directed towards either improving J_c by improving grain connectivity, or improving in-field performance by different methods.

Flux pinning and the upper critical field determine the magnitude of the current density J_c. The pinning mechanism has been widely studied for doped MgB_2 samples [3-12]. The critical current density of pure MgB_2 falls rapidly in high fields because of poor grain connectivity and lack of enough effective pinning centers. Introducing flux pinning centers through nanoparticle doping in bulk MgB_2 is an effective way to significantly improve the flux pinning. Many types of chemical doping have been examined for improving the J_c, the upper critical magnetic field, H_{c2}, and the irreversibility field, H_{irr} [13-15]. It has been found that chemical doping with nonmagnetic materials appears to be the simplest approach for increasing the ability of MgB_2 to carry large currents for practical applications. It has already been shown that J_c enhancement by more than one order of magnitude in high magnetic fields can be easily achieved with only a slight reduction in the critical temperature, T_c, through adding nanoparticles of certain elements and compounds, such as SiC, Si, and C, to MgB_2 [16–23].

The most important elementary interactions between vortices and pinning centers are the magnetic interaction and the core interaction [24-30]. The magnetic interaction arises from the interaction at surfaces between superconducting and non-superconducting material parallel to the applied field, but the magnetic interaction is usually very small in type–II superconductors with a high Ginzburg-Landau (GL) parameter κ. The core interaction arises from the locally distorted superconducting properties through the superconducting order parameter fluctuation, which is usually more effective in type–II superconductors. Two mechanisms of core pinning are predominant in type–II superconductors, i.e., δT_c and δl pinning. δT_c pinning is caused by the spatial variation of the GL coefficient α associated with disorder and variation in T_c, while the variations in the charge-carrier mean free path, l, near lattice defects are the main cause of δl pinning. A high κ

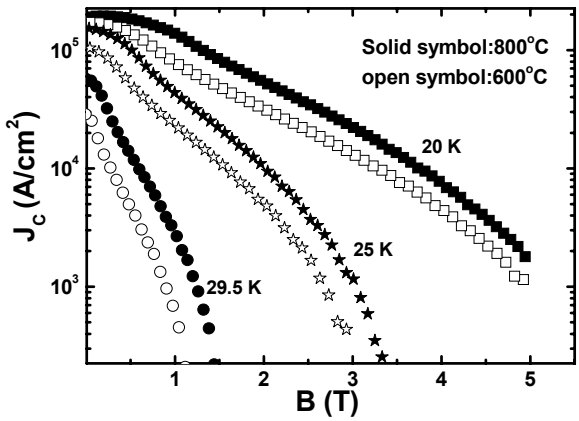

Figure 1. Magnetic and temperature dependences of the critical current density J_c for 600 and 800 °C reaction temperatures.

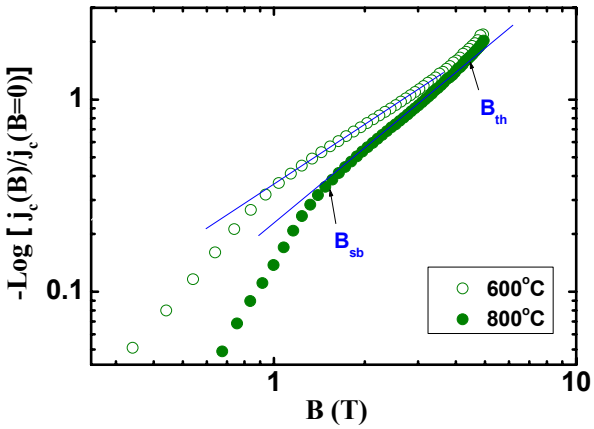

Figure 2. Double logarithmic plot of –log $[j_c(B)/j_c(0)]$ as a function of B at $T = 20$ (circles) and 26.5 K (rectangles) for the samples sintered at 600 (open symbols) and 800 °C (solid symbols). The crossover fields B_{sb} and B_{th} are shown by arrows for the sample at 26.5 K.

value of 26 has been reported [31] for MgB_2, indicating that magnetic interaction is negligible, and the core is more important.

In this paper we report the effects of the sintering temperature on the pinning mechanism and the flux activation energy of the 10 wt% malic-acid doped MgB_2. It was found that the δl pinning mechanism was dominant at low temperature, while at temperatures close to the critical temperature, δT_c pinning is effective. Our results suggest that by increasing sintering temperature the δT_c pinning contribution decreases, while the δl pinning effects increases. The results show that the flux-flow activation energy divided by Boltzmann's constant (U_o/k_B) increases by in the flux pinning potential.

2. Experiment

Boron powder, toluene, and 10 wt % malic acid ($C_4H_6O_5$) were fully mixed and sintered at 210 °C in order to decompose the malic acid. Then, the resultant powder was mixed with Mg, and dried and compressed into a pellet. The pellets were sintered at different temperatures in the range of 600 – 800 °C. The electrical resistivity was measured by a standard dc four-probe method on sintered bars with typical dimensions of 2.3 × 3.5 × 1.1 mm^3. All magnetic and transport measurements were performed using a physical properties measurement system (PPMS, Quantum Design). From the M(H) loops, the J_c was calculated using the Bean approximation, $J_c = 20\Delta M/(Va(1-a/3b))$, where a and b are the width and the length of the sample perpendicular to the applied field, respectively, V is the sample volume, and ΔM is the height of the M-H hysteresis loop.

The crystal structure was investigated by x-ray diffraction (XRD) [32]. It was observed that 10 wt% $C_4H_6O_5$ doped MgB_2 samples sintered at 600–900 °C seemed to be well-developed MgB_2 with a small amount of MgO, which is decreased by increasing sintering temperature.

3. Results and discussion

The resultant J_c(B,T) curves at various temperatures for samples sintered at 600 and 800 °C are shown in a double-logarithmic plot in figure 1. As can be seen from the plateau at low field, J_c initially has a weak dependence on the magnetic field. When the field is increased beyond a crossover field, it begins to decrease quickly.

At 4 T and 20 K, the J_c values for both samples are over 1×10^4 A/cm^2, more than one order of magnitude higher than for pure MgB_2 [25]. This is due to enhancement of flux pinning, which may be ascribed to C substitution into B sites. For all fields and temperatures lower than 29.5 K, the critical current density of samples sintered at 800 °C is higher than for those sintered at 600°C. This is in agreement with the increased grain connectivity, greater C substitution into the B sites, and decreasing MgO phase resulting from the higher temperature sintering.

In order to understand the critical current density results shown in figure 1, the vortex-pinning mechanism was investigated by using dependence of the crossover field in the framework of the collective theory, which has been derived by Blatter *et al*. [25], where J_c is field independent when the applied magnetic field is lower than the crossover field B_{sb} (the single vortex pinning regime). For $B > B_{sb}$ (small-bundle pinning regime), J_c(B) follows an exponential law,

$$J_c(B) \approx J_c(0)\exp[-(B/B_0)^{3/2}] \quad (1)$$

Where B_0 is a normalization parameter of the order of B_{sb} and $J_c(0)$ is the critical current density at zero field. When $B > B_{lb}$, the crossover field is between the small and the large vortex bundle regimes, this large-bundle pinning regime is governed by the power law $J_c(B) \propto B^{-\alpha}$, with α=3 for RE-123 (RE= rare earth elements) superconductor [25]. Figure 2 presents a double-logarithmic plot of – log $[J(B)/J(B=0)]$ as a function of applied magnetic field. At intermediate fields, Eq. (1) fits the experimental data of $J_c(B)$ very

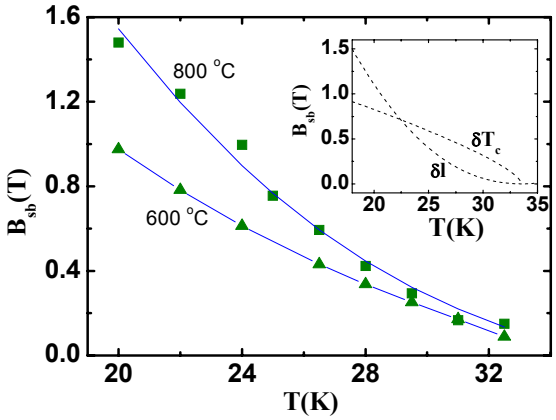

Figure 3. Temperature dependence of the crossover field B_{sb}. The solid curves are fits to eq. (3). Inset: The δT_c and δl pinning correspond to eq. (2).

well, while deviations from the fitting curves can be observed at both low and high fields.

B_{sb} indicates the crossover field from the single vortex-pinning regime to the small-bundle-pinning regime, while the deviation at high fields has been considered as the crossover field from small-bundle pinning to large-bundle pinning. The high-field deviation, however, is very close to the irreversibility line, which results from giant flux creep, so it is likely that the deviation at high field may instead result from large thermal fluctuations, which lead to the rapid decrease in J_c. This deviation is therefore denoted as B_{th} .

It was pointed out [25] that B_{sb} is proportional to the critical current density J_{sv} in the single vortex pinning regime. Griessen *et al*. [24] have found that for the δl pinning mechanism $J_{sv} \propto (1\text{-}t^2)^{5/2}(1+t^{2)\text{-}1/2}$, while for the δT_c pinning mechanism, $J_{sv} \propto (1\text{-}t^2)^{7/6}(1+t^2)^{5/6}$, where $t = T/T_c$. They have obtained the following expression for B_{sb}

$$B_{sb}(T) = B_{sb}(0)(1\text{-}t^2/1+t^2)^{\beta}, \quad (2)$$

where β = 2 and 2/3 for the δl and the δT_c pinning mechanisms, respectively. To investigate further the real pinning mechanism of the 10% malic-acid-doped MgB_2 samples, the B_{sb} data was analyzed using the following expression [33]

$$B_{sb}=P_1B_{sb}^{Tc}+P_2B_{sb}^{l}, \quad (3)$$

where B_{sb}^{Tc} and B_{sb}^{l} are the expressions for the δT_c and δl pinning, respectively. P_1 and P_2 are fitting parameters with $P_1+P_2 = 1$. The B_{sb} data obtained from J_c(B) was well described by eq. (3), as shown by the solid curves in figure 3.

In the inset of figure 3, the dashed curves indicate the δT_c and δl pinning mechanisms, corresponding to Eq. (2). The curve has a positive curvature in the δT_c pinning case, while the curvature associated with the δl pinning is negative. As is clear from figure 3, the $B_{sb}(T)$ behavior shows a negative curvature.

This rssults shows that the δl due to spatial fluctuations of the charge-carrier mean free path and δT_c pinning mechanisms due to the variation in T_c among the grains coexist at both temperatures. In order to compare the effects of the δT_c and δl pinning mechanisms, the P parameter was defined as $P=P_1B_{sb}^{Tc}/B_{sb}$ or $P=P_2B_{sb}^{l}/B_{sb}$,

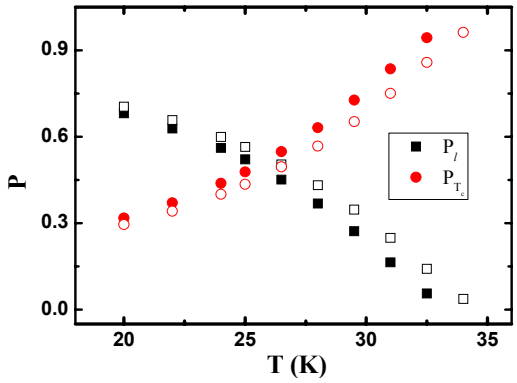

Figure 4. The δT_c and δl pinning contributions as functions of temperature. Open symbols: 600 °C. Solid symbols: 800 °C.

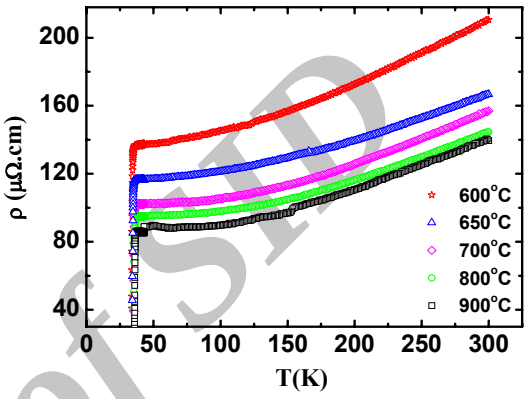

Figure 5. Temperature dependence of the resistivity of the 10 wt% malic-acid doped MgB_2 at different sintering temperatures and zero magnetic field.

which represent the δT_c and δl pinning effects, respectively.

The results of both pinning effect contributions are shown in figure 4. For both 600 and 800ºC reaction temperatures, the actual values of the pinning contribution are slightly different, while the trends in both the δT_c pinning and the δl pinning are the same. As can be seen in figure 4, results show that the δl pinning is the dominant mechanism at low temperature, but by increasing temperature, the δl pinning decreases, and the δT_c pinning increases. At the equivalence temperature, T_{eq} = 25.2 and 26.6 K for 800 and 600 ºC reaction temperatures, respectively, both pinning mechanisms have equal effects, and above these temperatures, the δT_c pinning is dominant. This result suggests that for temperatures close to T_c, the T_c fluctuation increases, and therefore, the δl pinning is suppressed completely. When the temperature is far below T_c, the T_c fluctuation disappears, and the δl pinning is dominant. Both malic acid-doped MgB_2 samples at sintered at 600°C and 800°C have the same trend in both the δl and δT_c pinning mechanisms. It was found that by increasing sintering temperature the δT_c pinning contribution decreases, while the δl pinning effects increase.

Figure 5 shows the temperature dependence of the resistivity of the 10 wt% malic-acid doped MgB_2 at different sintering temperatures and zero magnetic field.

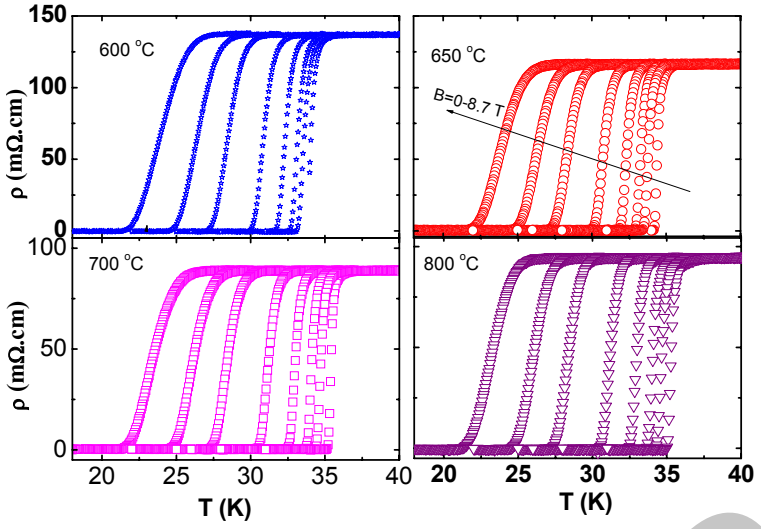

Figure 6. The electrical resistivity as a function of temperature in fields of 0-8.7 T for 10wt% malic acid doped MgB_2 sintered at 600, 650, 700, and 800 ºC.

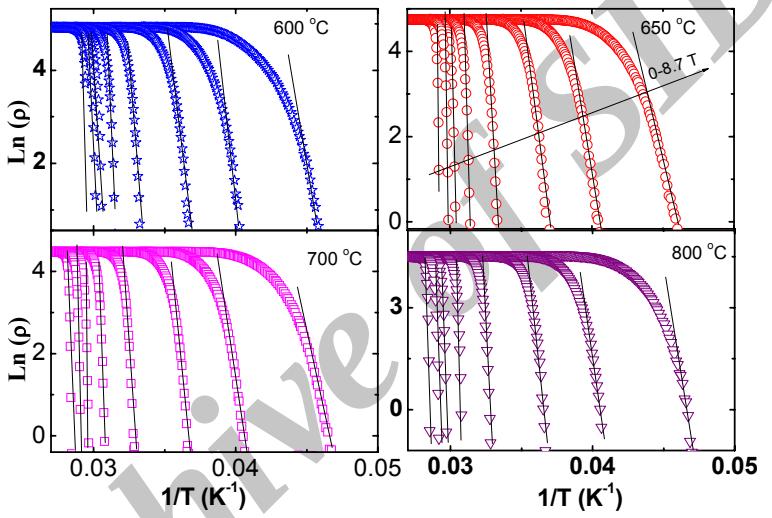

Figure 7. Arrhenius plot of the electrical resistivity for samples sintered at 600, 650, 700, and 800 ºC. The activation energy U_0 is given by the slopes from linear fitting, as shown.

As can be seen, the room temperature resistivity decreases by increasing sintering temperature. Thus, the impurity scattering is reduced as the sintering temperature increases, demonstrating the feasibility of improving the upper critical field [32]. Therefore, the highest upper critical fields were obtained for samples with lower sintering temperature, in this case, 600 ºC, as was found by Hossein et al. [32].

Figure 6 shows the resistivity as a function of magnetic field for samples sintered at 600, 650, 700, and 800 ºC in magnetic fields of 0-8.7 T. It can be seen from these curves that the critical temperature, T_c, decreases and the transition temperature width increases by increasing magnetic field. In large magnetic fields, due to flux penetration inside the grains, the onset part of the transition will be broadened. The amount of the broadening and the shift of T_c to lower temperature as a function of the magnetic field are proportional to the magnitude or strength of the pinning force.

Usually, the broadening of the lower parts of the resistive transition, $\rho(T) < 1\ \%\ \rho_n$ (where ρ_n is the resistivity in the normal state just above the transition), in a magnetic field is interpreted in terms of the dissipation of energy caused by the motion of vortices [34]. This interpretation is based on the fact that the resistance is caused by vortex creep, so that the $\rho(T)$ dependence is due to the thermally activated flux. In this region, the experimental results have been found to follow the Arrhenius relation

$$\rho(T,B) = \rho_o \exp[-U_o/k_BT] \quad (4)$$

Here, U_0 is the flux-flow activation energy, which can be obtained from the slope of the linear part of an Arrhenius plot, and ρ_0 is a field-independent pre-exponential factor. Activation energy for the broadened transition usually is independent of the temperature, and it can be obtained from the slope of the linear part of the ln ρ *vs.* $1/T$ curves, which are shown in figure 7 for different sintering temperatures.

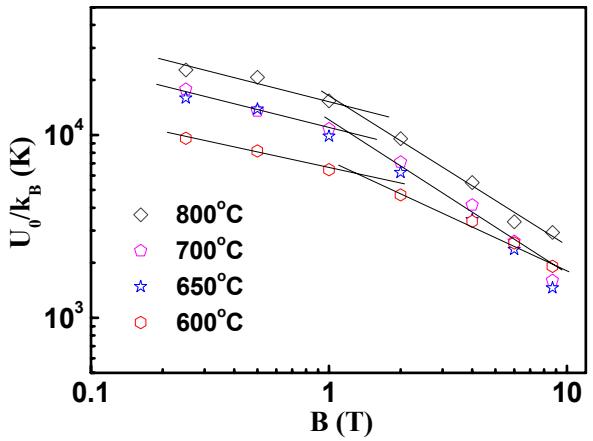

Figure 8. Magnetic field dependence of the activation energy U_0 for MgB_2 superconductor doped with 10wt% malic acid for sintering temperatures of 600- 800 ºC.

Figure 8 presents the obtained flux pinning energy, U_0, from the above fitting for different magnitudes of field for samples sintered at temperatures of 600, 650, 700, and 800 °C. It is clear from figure 8 that the activation energy increases by increasing sintering temperature. As can be seen for each sample, the flux pinning energy decreases by increasing applied magnetic field. The value of U_0 in high field for the malic acid doped MgB_2 is roughly 2000 K that is 10 and 5 times larger than that of Bi2223 [35] and Bi2212 [34], respectively. This indicates that the malic acid doped MgB_2 has a very much stronger pinning than that of Bi2223 and Bi2212 superconductors.

It has been reported that the pinning potential of bismuth strontium calcium copper oxide (BSCCO) crystals exhibits a power-law dependence on magnetic field, $U_0(H) \approx H^n$, with $n = 1/2$ for $H < 5$ T and $n = 1/6$ for $H > 5$ T for $H//c$ [34,35]. We have fitted this power law relation for U_0 versus H for each sample. The values of n have been obtained to be roughly 0.76 ± 0.02 in H > 1 T for sintering temperatures larger than 600 °C and n = 0.52 for the sintering temperature of 600 °C. However, for H ≤ 1 T, n does not depend on the sintering temperature and has the value 0.28±0.04.

In conclusion, we have found that the δl due to spatial fluctuations of the charge-carrier mean free path and δT_c pinning mechanisms due to the variation in T_c,coexist at both temperatures and both pinning mechanism contributions are strongly temperature dependent.The δl pinning mechanism is dominant at low temperature in 10 wt% malic-acid doped MgB_2 which is sintered at different temperatures, while at temperatures close to the critical temperature, δT_c pinning is effective. Our results suggest that the δT_c pinning contribution decreases while the δl pinning effects increases by increasing sintering temperature. The results show that U_o/k_B increases by increasing sintering temperature, which suggests an increase in the flux pinning potential

References

1. J Nagamatsu, N Nakagawa, Y Zenitani, and J Akimitsu, *Nature* **410** (2001) 63.
2. C Buzea, and T Yamashita, *Supercond. Sci. Technol.* **14** (2001) R115.
3. D C Larbalestier, M O Rikel, L D Cooley, A A Polyanskii, J Y Jiang, S Patnaik, X Y Cai, D M Feldmann, A Gurevich, A A Squitieri, M T Naus, C B Eom, E E Hellstrom, R J Cava, K A Regan, N Rogado, M A Hayward, T He, J S Slusky, P Khalifah, K Inumaru, and M Haas, *Nature* **410** (2001) 186.
4. Hyeong-Jin Kim, W N Kang, Eun-Mi Choi, Mun-Seog Kim, Kijoon H P Kim, and Sung-IK Lee, *Phys. Rev. Lett.* **87** (2001) 087002.
5. Mun-Seog Kim, C U Jung, Min-Seok Park, S Y Lee, Kijoon H P Kim, W N Kang, and Sung-Ik Lee, *Phys. Rev.* B **64** (2001) 012511.
6. M J Qin, X L Wang, H K Liu, and S X Dou, *Phys. Rev.* B **65** (2002) 132508.
7. M Eisterer, M Zehetmayer, and H W Weber, *Phys. Rev. Lett.* **90** (2003) 247002.
8. S Y Xu, Qi Li, E Wertz, Y F Hu, A V Pogrebnyakov, X H Zeng, X X Xi, and J M Redwing, *Phys. Rev.* B **68** (2003) 224501.
9. H Kitaguchi, A Matsumoto, H Kumakura, T Doi, H Yamamoto, K Saitoh, H Sosiati, and S Hata, *Appl. Phys. Lett.* **85** (2004) 2842.
10. S X Dou, O Shcherbakova, W K Yeoh, J H Kim, S Soltanian, X L Wang, C Senatore, R Flukiger, M Dhalle, O Husnjak, and E Babic, *Phys. Rev. Lett.* **98** (2007) 097002.
11. Z X Shi, A K Pradhan, M Tokunaga, K Yamazaki, T Tamegai, Y Takano, K Togano, H Kito, and H Ihara, *Phys. Rev.* B **68** (2003) 104514.
12. Z X Shi, J Wang, H Lv, and T Tamegai, *Physica* C **449** (2006) 104.
13. W J Feng, T D Xia, T Z Liu, W J Zhao, and Z Q Wei, *Physica* C **425** (2005) 144.
14. V P S Awana, M Isobe, K P Singh, E Takayama Muromachi, and H Kishan, *Supercond. Sci. Technol.* **19** (2006) 551.
15. J H Kim, S X Dou, M S A Hossain, X Xu, J L Wang, D Q Shi, T Nakane, and H Kumakura, *Supercond. Sci. Technol.* **20** (2007) 715.
16. S X Dou, S Soltanian, J Horvat, X L Wang, S H Zhou, M Ionescu, H K Liu, P Munroe, and M Tomsic, *Appl. Phys. Lett.* **81** (2002) 3419.
17. X L Wang, S H Zhou, M J Qin, P R Munroe, S Soltanian, H K Liu, and S X Dou, *Physica* C **385** (2003) 461.
18. X L Wang, S Soltanian, M James, M J Qin, J Horvat, Q W Yao, H K Liu, and S X Dou, *Physica* C **408** (2004) 63.
19. S Soltanian, J Horvat, X L Wang, P Munroe, and S X Dou, *Physica* C **390** (2003) 185.
20. R H T Wilke, S L Bud'ko, P C Canfield, D K

Finnemore, R J Suplinskas, and S T Hannahs, *Phys. Rev. Lett*. **92** (2004) 217003.
21. B J Senkowicz, J E Giencke, S Patnaik, C B Eom, E E Hellstrom, and D C Larbalestier, *Appl. Phys. Lett*. **86** (2005) 202502.
22. V Braccini, A Gurevich, J E Giencke, M C Jewell, C B Eom, D C Larbalestier, A Pogrebnyakov, Y Cui, B T Liu, Y F Hu, J M Redwing, Qi Li, X X Xi, R K Singh, R Gandikota, J Kim, B Wilkens, N Newman, J Rowell, B Moeckly, V Ferrando, C Tarantini, D Marré, M Putti, C Ferdeghini, R Vaglio, and E Haanappel, *Phys. Rev*. B **71** (2004) 012504.
23. S K Chen, M Wei, and J L MacManus-Driscoll, *Appl. Phys. Lett*. **88** (2006) 192512.
24. R Griessen, Wen Hai-hu, A J J van Dalen, B Dam, J Rector, and H G Schnack, *Phys. Rev. Lett*. **72** (1994) 1910.
25. G Blatter, M V Feigel'man, V B Geshkenbein, A I Larkin, and V M Vinokur, *Rev. Mod. Phys*. **66** (1994) 1125.
26. Roger Wördenweber, *Rep. Prog. Phys*. **62** (1999) 187.
27. E V Thuneberg, *Cryogenics* **29** (1989) 236.
28. E V Thuneberg, J Kurkijarvi, and D Rainer, *Phys. Rev. Lett*. **48** (1982) 1853.
29. C J van der Beek, and P H Kes, *Phys. Rev*. B **43** (1991) 13 032.
30. P H Kes, *Physica* C **185-189** (1991) 288.
31. D K Finnemore, J E Ostenson, S L Bud'ko, G Lapertot, and P C Canfield, *Phys. Rev. Lett*. **86** (2001) 2420
32. M S A Hossain, J H Kim, X Xu, X L Wang, M Rindfleisch, M Tomic, M D Sumption, E W Collings, and S X Dou, *Supercond. Sci. Technol*. **20** (2007) L51.
33. S R Ghorbani, X L Wang, S X Dou, Sung-Ik Lee, and M S A Hossain, *Phys. Rev*. B **78** (2008) 184502.
34. T M Palstra, B Batlogg, R B van Dover, L F Schneemeyer, and J V Waszchak, *Phys. Rev*. B **41** (1990) 6621.
35. X L Wang, A H Li, S Yu, S Ooi, and K Hirata, C T Lin, E W Collings, M D Sumption, and M Bhatia, S Y Ding, S X Do, *J. Appl. Phys*. **97** (2005) 10B114.